Earth Planets Space, **60**, 773–779, 2008

A conservative and non-oscillatory scheme for Vlasov code simulations

Takayuki Umeda

Solar-Terrestrial Environment Laboratory, Nagoya University, Nagoya, Aichi 464-8601, Japan

(Received September 25, 2007; Revised February 28, 2008; Accepted April 9, 2008; Online published August 4, 2008)

A new numerical positive interpolation technique for conservation laws and its application to Vlasov code simulations are presented. In recent Vlasov simulation codes, the Vlasov equation is solved based on the numerical interpolation method because of its simplicity of algorithm and its ease of programming. However, a large number of grid points are needed in both configuration and velocity spaces to suppress numerical diffusion. In this paper we propose a new high-order interpolation scheme for Vlasov simulations. The current scheme is non-oscillatory and conservative and is well-designed for Vlasov simulations. This is compared with the latest interpolation schemes by performing one-dimensional electrostatic Vlasov simulations.
Key words: Vlasov equation, hyperbolic equation, numerical interpolation, conservation laws.

1. Introduction

Kinetic simulations are essential approaches to the study of nonlinear microscopic processes in space plasmas. Numerical methods used in these kinetic simulations fall into two groups. One is particle-in-cell simulation, which follows the motions of individual particles in a self-consistent electromagnetic field. However, a limitation on the number of particles gives rise to numerical thermal fluctuations. Another approach is Vlasov simulation, which follows the spatial and temporal development of distribution functions in the position-velocity phase space. Both particle-in-cell and Vlasov codes have advantages and disadvantages. An advantage of Vlasov codes is that thermal fluctuations, which are strongly enhanced in particle-in-cell simulations, can be suppressed. However, the particle-in-cell simulation techniques are well-developed, while numerical techniques for Vlasov simulations are still being worked out.

Recent Vlasov codes use transformation (spectral) schemes (Shoucri and Gagne, 1976; Klimas, 1983; Eliasson, 2003) or the splitting scheme (Cheng and Knorr, 1976; Gagne and Shoucri, 1977). The splitting scheme is widely used because of the simplicity of its algorithms and ease of programming (Utsumi *et al*., 1998; Nakamura and Yabe, 1999; Sonnendrucker *et al*., 1999; Filbet *et al*., 2001; Filbet and Sonnendrucker, 2003; Pohn *et al*., 2005; Umeda *et al*., 2006). With the splitting scheme the integration of distribution functions reduces to a numerical interpolation. However, a large number of grid points are needed in both configuration and velocity spaces to maintain the energy and mass conservations and to suppress numerical diffusion.

Recently, a high-order semi-Lagrangian scheme, called the Constrained Interpolation Profile (CIP) scheme (Yabe *et al*., 2001), was implemented in Vlasov codes (Utsumi *et al*., 1998; Nakamura and Yabe, 1999) where it was used for a simulation of harmonic Langmuir waves (Umeda *et al*., 2003). Although numerical diffusion in the CIP scheme is very low, this scheme needs to solve the equations for partial derivatives or integrals of a distribution function f, i.e., $\nabla_x f$ and $\nabla_v f$, or $\int f \mathrm{d}x$, $\int f \mathrm{d}v$, and $\int\int f \mathrm{d}x\mathrm{d}v$. The additional storage of partial derivatives or integrals makes it difficult to apply the CIP scheme to five- or six-dimensional phase-space Vlasov codes. It is also demonstrated that multi-dimensional CIP-type schemes become oscillatory, generating a positive gradient in a velocity distribution function that causes a non-physical instability (Umeda *et al*., 2006).

Meanwhile, Filbet *et al*. (2001) developed a high-order conservative scheme called the Positive and Flux Conservative (PFC) scheme. Although numerical diffusion in conservative schemes is somewhat higher than that in non-conservative schemes, the PFC scheme appears to be more efficient for Vlasov simulations of several classical problems of plasma physics (Filbet and Sonnendrucker, 2003). Umeda *et al*. also demonstrated that Vlasov codes with conservative schemes provide better characteristics for the mass and energy conservations (Umeda *et al*., 2006). It is a new trend to implement conservative interpolation schemes in Vlasov codes. A new conservative scheme without splitting has also been proposed (Elkina and Buchner, 2005).

Characteristics of the recent Vlasov codes for classical problems of plasma physics, such as linear and nonlinear Landau damping, linear growth, and saturation of weak beam-plasma interactions, have been studied by many authors (Filbet and Sonnendrucker, 2003; Pohn *et al*., 2005; Arber and Vann, 2002; Mangeney *et al*., 2002). In contrast, Umeda *et al*. (2006) compared recent interpolation schemes for long-time and nonlinear kinetic processes in space plasmas. They concluded that non-oscillatory, shape-preserving, conservative, positivity-preserving, low numerical diffusion, and computer-memory saving are necessary properties of interpolation schemes for Vlasov simulations.

In this study we propose a new positive interpolation

scheme for conservation laws that is a modified version of the PFC scheme and has all the properties listed above. The purpose of this paper is twofold. The first is to give a detailed numerical procedure for the present scheme, and the second is to compare the present scheme with the latest non-conservative and conservative schemes by performing one-dimensional (1D) Vlasov simulations.

The paper is structured as follows. The present scheme is introduced in Section 2. Numerical solutions to the 1D linear advection equation and results of Vlasov simulations with the present and other high-order interpolation schemes are compared in Section 3. A discussion and conclusion are presented in Section 4.

2. Numerical Procedure

We adopt here a conservative semi-Lagrangian scheme used by Filbet *et al*. (2001). The starting point is a solution to the linear advection equation

$$\frac{\partial f}{\partial t} + v\frac{\partial f}{\partial x} = 0. \tag{1}$$

Let us consider an arbitrary piecewise function $g(x)$ that approximates a profile f_i. The profile f_i is defined as the integral of the piecewise function $g(x)$ as shown in Fig. 1,

$$f_i = \int_{i-\frac{1}{2}}^{i+\frac{1}{2}} g(x)\mathrm{d}x. \tag{2}$$

A solution to the advection equation (2) then takes the following conservative form

$$f_i^{t+\Delta t} = f_i^t + U_{i-\frac{1}{2}}(\nu) - U_{i+\frac{1}{2}}(\nu), \tag{3}$$

where U is a numerical flux, v is a constant advection velocity, and $\nu = -v\frac{\Delta t}{\Delta x}$ is the CFL number which is taken in the opposite direction to v. Note that Eq. (3) corresponds to the general solution to the linear advection equation (2),

$$f(t + \Delta t, i\,\Delta x) = f(t, i\,\Delta x - v\Delta t). \tag{4}$$

As an example, the third-order upwind-biased Lagrange polynomial interpolation is considered,

$$\begin{aligned} f(x) = {} & f_i + (x-i)(f_i - f_{i-1}) \\ & + (x-i)(1+x-i)(2+x-i)\frac{f_{i-1} - 2f_i + f_{i+1}}{6} \\ & + (x-i)(1+x-i)(1-x+i)\frac{f_{i-2} - 2f_{i-1} + f_i}{6}. \end{aligned} \tag{5}$$

Here $\Delta x = 1$ is assumed for simplicity. Note that the function $f(x)$ does not correspond to $g(x)$ since $f_i \equiv f(x = i)$ is defined as the integral of g. To take the conservative form (3), numerical flux is given as

$$\begin{aligned} U_{i+\frac{1}{2}}(\nu) = {} & \nu f_i + \nu(1-\nu)(2-\nu)\frac{f_{i+1} - f_i}{6} \\ & + \nu(1-\nu)(1+\nu)\frac{f_i - f_{i-1}}{6}, \end{aligned} \tag{6}$$

where $\nu = i - x$. Since the numerical flux is also defined as

$$U_{i+\frac{1}{2}}(\nu) \equiv \int_{i+\frac{1}{2}-\nu}^{i+\frac{1}{2}} g(x)\mathrm{d}x, \tag{7}$$

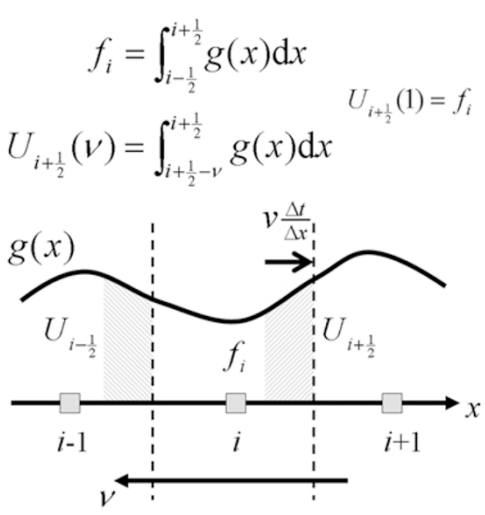

Fig. 1. Schematic illustration showing a procedure for solving the advection equation with a conservative scheme. The profile is advanced by Eq. (1).

Eq. (6) is easily obtained by the following constraints, $U_{i+\frac{1}{2}}(0) = 0$, $U_{i+\frac{1}{2}}(1) = f_i$, $U_{i+\frac{1}{2}}(2) = f_{i-1}$, and $U_{i+\frac{1}{2}}(-1) = -f_{i+1}$.

For a negative velocity $v < 0$ we use upwind-biased points f_{i-1}, f_i, f_{i+1}, and f_{i+1}. Thus, the numerical flux is given as

$$\begin{aligned} U_{i+\frac{1}{2}}(\nu) = {} & \nu f_{i+1} + \nu(1+\nu)(2+\nu)\frac{f_i - f_{i+1}}{6} \\ & + \nu(1-\nu)(1+\nu)\frac{f_{i+1} - f_{i+2}}{6}. \end{aligned} \tag{8}$$

It is well-known that a high-order scheme is oscillatory and generates new extrema, i.e., local maximum or minimum (Godunov, 1959). Thus, a flux limiter or slope corrector has been introduced to suppress the numerical oscillations (Filbet *et al*., 2001). Equation (6) is rewritten as

$$\begin{aligned} U_{i+\frac{1}{2}}(\nu) = {} & \nu f_i + \nu(1-\nu)(2-\nu)\frac{L_i^{(+)}}{6} \\ & + \nu(1-\nu)(1+\nu)\frac{L_i^{(-)}}{6}, \end{aligned} \tag{9}$$

where

$$L_i^{(+)} = \begin{cases} \min[2(f_i - f_{\min}), (f_{i+1} - f_i)] \\ \qquad \text{if } f_{i+1} \geq f_i \\ \max[2(f_i - f_{\max}), (f_{i+1} - f_i)] \\ \qquad \text{if } f_{i+1} < f_i \end{cases} \tag{10}$$

$$L_i^{(-)} = \begin{cases} \min[2(f_{\max} - f_i), (f_i - f_{i-1})] \\ \qquad \text{if } f_i \geq f_{i-1} \\ \max[2(f_{\min} - f_i), (f_i - f_{i-1})] \\ \qquad \text{if } f_i < f_{i-1} \end{cases} \tag{11}$$

In the PFC scheme proposed by Filbet *et al*. (2001), the maximum and minimum values of the piecewise polynomial $f_{\max}$ and $f_{\min}$ are given by $f_{\max} = f_\infty \equiv \max_{i=1\sim N_x}[f_i]$, and $f_{\min} = 0$, respectively. This means that the maximum value of the profile decreases. To allow the

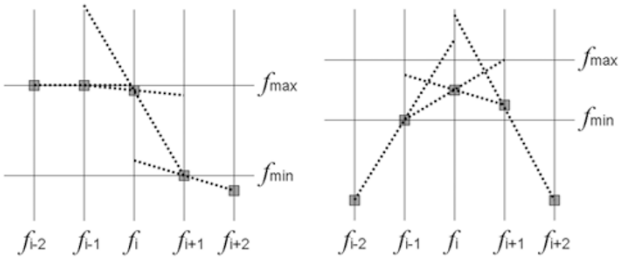

Fig. 2. Detection of discontinuities and local extrema.

profile to rise uncontrollably, Schmitz and Grauer modified the limiter using $f_{\max} = \infty$ (Schmitz and Grauer, 2006). In these schemes, however, one can find that the profile is not necessarily non-oscillatory and has a local maximum and/or minimum. Here, the concept of a "non-oscillatory" scheme is not to generate new extrema numerically but to keep already-existing extrema.

As a non-oscillatory scheme, we use the following maximum and minimum values for the piecewise polynomial,

$$f_{\max}=\max\left[f_{\max 1},\, f_{\max 2}\right],$$
$$f_{\min}=\min\left[f_{\min 1},\, f_{\min 2}\right],$$

where

$$f_{\max 1}=\max\left[\max[f_{i-1},\, f_i],\, \min[2f_{i-1}-f_{i-2},\, 2f_i-f_{i+1}]\right],$$
$$f_{\max 2}=\max\left[\max[f_{i+1},\, f_i],\, \min[2f_{i+1}-f_{i+2},\, 2f_i-f_{i-1}]\right],$$
$$f_{\min 1}=\min\left[\min[f_{i-1},\, f_i],\, \max[2f_{i-1}-f_{i-2},\, 2f_i-f_{i+1}]\right],$$
$$f_{\min 2}=\min\left[\min[f_{i+1},\, f_i],\, \max[2f_{i+1}-f_{i+2},\, 2f_i-f_{i-1}]\right].$$

We can easily detect both extrema and discontinuities with the above procedure, as shown in Fig. 2. It is noted that we can preserve positivity if we use

$$f_{\min} = \max\left[0, \min[f_{\min 1},\, f_{\min 2}]\right].$$

Thus, the present scheme is a modified version of the PFC scheme.

3. Numerical Tests

3.1 Linear advection

We solved the 1D linear advection equation $\frac{\partial f}{\partial t}+v\frac{\partial f}{\partial x}=0$ with a constant velocity v numerically. We used rectangular and sinusoidal waves as initial profiles and applied the forth-order Monotone Upstream-centered Scheme for Conservation Laws (MUSCL) scheme (Yamamoto and Daiguji, 1993), the fifth-order Weighted Essentially Non-Oscillatory (WENO) scheme (Jiang and Shu, 1996), the third-order CIP (CIP-3) scheme (Yabe *et al*., 2001), the rational CIP (R-CIP) scheme (Xiao *et al*., 1999), and the present scheme. Note that the Euler time-integration scheme was used for both the MUSCL and WENO schemes. We imposed the periodic boundary condition. Figure 3 shows results of the numerical tests for the linear advection with the CFL number $v\frac{\Delta t}{\Delta x}=0.1$. The left and right panels correspond to the results with the rectangular and sinusoidal waves, respectively. The solid lines show the profiles at the tenth cycle (i.e., time step = 8000), while the dashed lines show the initial profiles.

The MUSCL and WENO schemes show the best property for the linear advection of the rectangular wave because these are called "shock capturing" schemes. For the sinusoidal wave, on the other hand, we found a modification of the profile during the linear advection. The MUSCL scheme artificially rectangularizes profiles to keep monotonicity, while the sinusoidal wave is strongly amplified with the WENO scheme. Note that the amplification can be suppressed with higher-order Runge-Kutta time-integration schemes. However, we found that the property for the linear advection become worse with the Runge-Kutta schemes than with the Euler scheme. Although the MUSCL and WENO schemes are well-designed for shocks and discontinuities, they are not necessarily appropriate for the advection of sinusoidal waves.

The CIP-3 scheme gives the best result for the linear advection of the sinusoidal wave, whereas this scheme generates spurious oscillations for the rectangular wave. One can suppress the spurious oscillations using a rational interpolant instead of the cubic polynomial interpolant (Xiao *et al*., 1999). However, the amplitude of the sinusoidal wave with the R-CIP scheme becomes lower than that with the CIP-3 scheme, which means that R-CIP scheme is more diffusive than the CIP-3 scheme.

The results with the present scheme look very similar to those with the R-CIP scheme. However, one may think that the present scheme is much more diffusive than the CIP-3 and R-CIP schemes. We emphasize that the both CIP-3 and R-CIP schemes use twice as much computer memory space as the present scheme because the CIP-type schemes need to store partial derivatives or integrals of the profile. As shown in Fig. 3, the results with the present scheme improve to being better than the results with the R-CIP scheme when we use 1.5-fold more computer memory space for the 1D problem.

In summary, the MUSCL and WENO schemes, which are commonly used in fluid simulations, are useful for keeping rectangular shapes or discontinuous profiles. Note that the rectangular waveforms with the MUSCL and WENO schemes are preserved for a longer time. Meanwhile, the CIP-type and present schemes are based on the semi-Lagrangian method in which profiles are interpolated with a cubic polynomial or a rational functions. Thus, these schemes are good at the advection of continuous profiles. However, the amplitude of sinusoidal waves with the CIP, R-CIP, and the present schemes gradually decreases with more timesteps.

3.2 Vlasov simulations

The Vlasov equation is solved with the time-advance algorithm called the splitting method (Cheng and Knorr, 1976), in which the Vlasov equation without magnetic fields splits into the following two advection equations:

$$\frac{\partial f_s}{\partial t}+v_x\frac{\partial f_s}{\partial x}=0, \tag{12}$$

$$\frac{\partial f_s}{\partial t}+\frac{q_s}{m_s}E_x\frac{\partial f_s}{\partial v_x}=0, \tag{13}$$

where the subscript s represents particle species (e.g., electrons and ions). The time advance of distribution functions $f_s(x, v_x)$ is carried out by shifting the distribution function

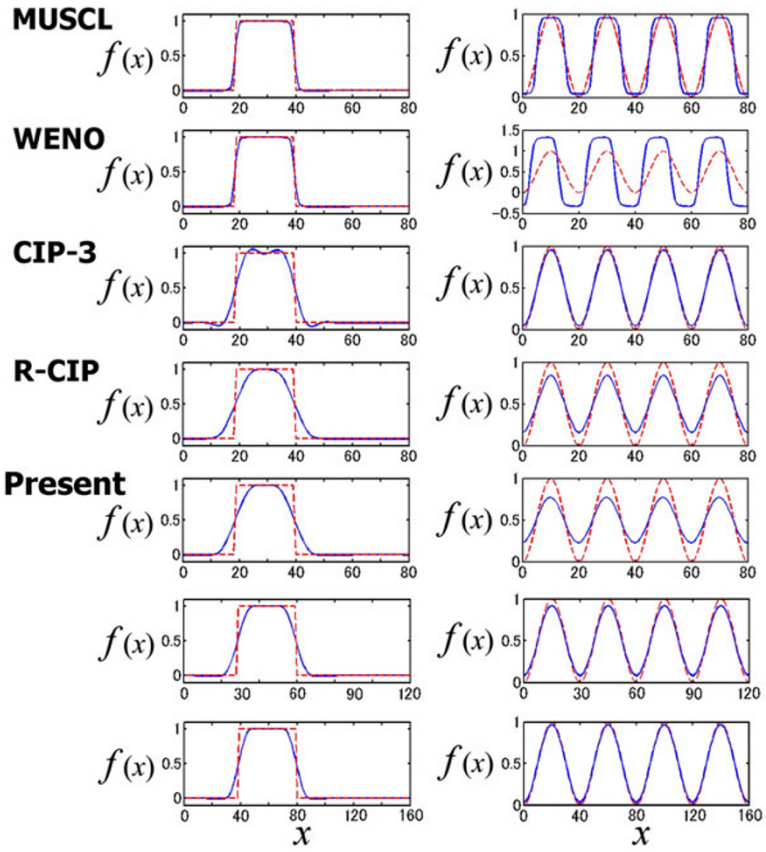

Fig. 3. Numerical test results for the linear advection. The one-dimensional linear advection equation is solved with the forth-order Monotone Upstream-centered Scheme for Conservation Laws (MUSCL) scheme, the fifth-order Weighted Essentially Non-Oscillatory (WENO) scheme, the third-order Constrained Interpolation Profile (CIP-3) scheme, the rational CIP (R-CIP) scheme, and the present scheme. A rectangular wave is used as the initial profile in the left panels, while a sinusoidal wave is used as the initial profile in the right panels. The solid lines show profiles after ten cycles (8000 time steps with the CFL number 0.1), and the dashed lines show the initial profiles. For the present scheme, results with different number of cells (120 cells with 12000 time steps and 160 cells with 16000 time steps) are also presented.

in the x direction (12) with the time step $\Delta t/2$, computing spatial profiles of charge density ρ by integrating the distribution functions over v_x, thereby solving Poisson's equation to obtain spatial profiles of electric field E_x, shifting the distribution function in the v_x direction (13) with the time step Δt, and again shifting the distribution function in the x direction (12) with the time step $\Delta t/2$. We used the forth-order MUSCL scheme, the fifth order WENO scheme, the CIP-3 scheme, the R-CIP scheme, and the present scheme to solve the above two advection equations.

We have examined the long-time nonlinear evolution of the electron two-stream instability to study the characteristics of the different interpolation schemes for a strongly nonlinear problem. Note that classical problems of plasma physics, which are usually done as benchmark tests for Vlasov codes, are not focused on in this paper because there is no critical difference between conventional and recent schemes. In fact, the present scheme gives almost the same result as the PFC scheme (Filbet *et al.*, 2001) in the benchmark tests for linear and nonlinear Landau damping, and linear growth and saturation of weak beam-plasma interactions, since the present scheme is a modified (i.e., non-oscillatory) version of the PFC scheme.

We assume two electron beams having equal density 0.5 and equal initial thermal velocity $V_t = 0.3|V_d|$. The two electron beams drift along the ambient magnetic field with a drift velocity $V_d = \pm 3.3 V_t$. The number of cells in the x direction is $N_x = 256$. The number of cells in the v direction is $N_v = 512$, with $v_{max} = 5.0V_d$, $v_{min} = -5.0V_d$. The grid spacing is equal to $\Delta x = 0.5V_d/\omega_{pe}$, and the time step is equal to $\omega_{pe}\Delta t = 0.01$. In the x direction we imposed the periodic boundary condition. In the v direction we imposed the open boundary condition where constant numerical fluxes $\frac{q}{m}E_x(x_i)\frac{\Delta t}{\Delta x}f(x_i, v_{max})$ and $\frac{q}{m}E_x(x_i)\frac{\Delta t}{\Delta x}f(x_i, v_{min})$ are assumed while outgoing perturbations of distribution functions are perfectly absorbed.

Figure 4 shows results of the numerical tests. In the left, middle, and right panels, we plot electron phase-space densities $f(x, v)$ at $\omega_{pe}t = 50$, $\omega_{pe}t = 200$, and $\omega_{pe}t = 1000$, respectively. The velocity and position are normalized by V_d and V_d/ω_{pe}, respectively. For a long run-time, nonlinear evolution, the electron two-stream instability develops to form solitary electron phase-space holes. We started the test runs under exactly the same initial conditions. The profiles of phase-space distribution functions at the early nonlinear stage ($\omega_{pe}t = 50$) are almost the same except for the case with the MUSCL scheme. The profiles of phase-space distribution functions at $\omega_{pe}t = 200$ are also similar, giving three or four phase-space density holes. On the other hand, the profiles of phase-space distribution functions at

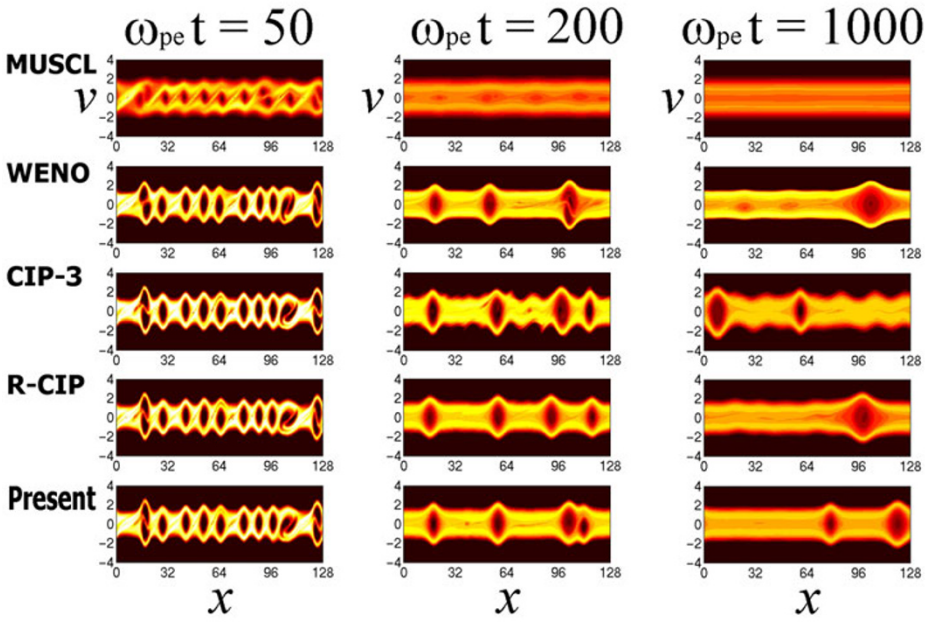

Fig. 4. Results for Vlasov simulations of the electron two-stream instability. The Vlasov equation is solved with the forth-order Monotone Upstream-centered Scheme for Conservation Laws (MUSCL) scheme, the fifth-order Weighted Essentially Non-Oscillatory (WENO) scheme, the third-order Constrained Interpolation Profile (CIP-3) scheme, the rational CIP (R-CIP) scheme, and the present scheme. (left) Electron phase-space densities $f(x, v)$ at $\omega_{\rm pe}t = 50$. (middle) Electron phase-space densities $f(x, v)$ at $\omega_{\rm pe}t = 200$. (right) Electron phase-space densities $f(x, v)$ at $\omega_{\rm pe}t = 1000$. The velocity and position are normalized by $V_{\rm d}$ and $V_{\rm d}/\omega_{\rm pe}$, respectively.

$\omega_{\rm pe}t = 1000$ are very different from each other because of the accumulation of numerical error. It is noted that we have performed several runs with more grid points (2048, and 4096) in the velocity space. We found two electron phase-space holes at the final state ($\omega_{\rm pe}t = 1000$) in the runs with WENO, CIP, R-CIP, and the present schemes, implying that the coalescence of phase-space holes is stimulated by numerical error in the runs with WENO and R-CIP schemes shown in Fig. 4.

The MUSCL scheme artificially "rectangularizes" a profile that generates a very sharp gradient in velocity distribution functions. Since the rectangularization in the velocity distribution function causes strong growth and damping of waves in a resonant velocity range, an equilibrium state can be numerically broken. Thus, there is not any coherent potential structure $\omega_{\rm pe}t = 1000$ with the MUSCL scheme. One may find that TVD schemes widely used in the computational fluid dynamics are not necessarily effective for Vlasov simulation.

In Fig. 5 we show time histories of electric field energy $\mathcal{E}_{\rm f} = \sum |E_x|^2$, kinetic energy $\mathcal{E}_{\rm k} = \sum v^2 |f|$, total energy $\mathcal{E} = \mathcal{E}_{\rm f} + \mathcal{E}_{\rm k}$, momentum $\mathcal{M} = \sum v|f|$, L1 norm (total density) $\mathcal{L}_1 = \sum |f|$, L2 norm $\mathcal{L}_2 = \sum |f|^2$, entropy $\mathcal{S} = -\sum |f| \ln |f|$, and the maximum and minimum values of the distribution functions obtained with the fifth-order WENO, CIP-3, R-CIP, and the present schemes. Here, $\sum f$ means that the phase-space distribution function $f(x, v)$ is integrated over x and v. The quantities $\mathcal{E}_{\rm k}$, $\mathcal{E}$, $\mathcal{L}_1$, $\mathcal{L}_2$, and $\mathcal{S}$ are plotted as deviations from the initial values. The momentum, L1 and L2 norms, and entropy are normalized by their initial values, whereas the energy quantities are normalized by the initial total energy.

In the case with the CIP-3 scheme, there are spurious oscillations in the phase-space distribution function as seen at $\omega_{\rm pe}t = 200$ and 1000 in Fig. 4. The CIP scheme numerically generates apparent overshoots or undershoots, which results in a positive gradient in the velocity distribution function. Waves are excited by an instability caused by the positive gradient in the velocity distribution function, which is, however, a non-physical process. The spurious oscillations in the distribution function can be suppressed using a rational function. The properties of density, energy, and momentum conservations with the R-CIP scheme become better than those with the CIP scheme. However, the R-CIP scheme is not necessarily non-oscillatory in multi-dimensional systems. Thus, we found weak oscillations in the phase-space distribution function at $\omega_{\rm pe}t = 1000$. Note that the value of the distribution function can be also negative with the CIP and R-CIP schemes, as seen in the history of $f_{\rm min}$ in Fig. 5.

Since the WENO scheme is a higher-order non-oscillatory scheme, the WENO scheme provides better properties for the momentum and energy conservations than the CIP and R-CIP schemes. However, the total density (L1 norm) is not conserved in Fig. 5, although the WENO scheme is a conservative scheme. This is simply because we have computed the L1 norm by $\sum |f|$ instead of $\sum f$. In other words, $\sum f$ is almost constant, but $\sum |f|$ varies in time. We found the increase in the L1 norm for $\omega_{\rm pe}t = 50 \sim 200$, when a strong nonlinear wave-particle interaction takes place in the $x - v$ phase space and the distribution function take a negative value, as seen in the history of $f_{\rm min}$. Since the positivity is not preserved with the WENO scheme, the distribution function can take a negative value by the strong modification of the distribution function, which may distort the energy and momentum con-

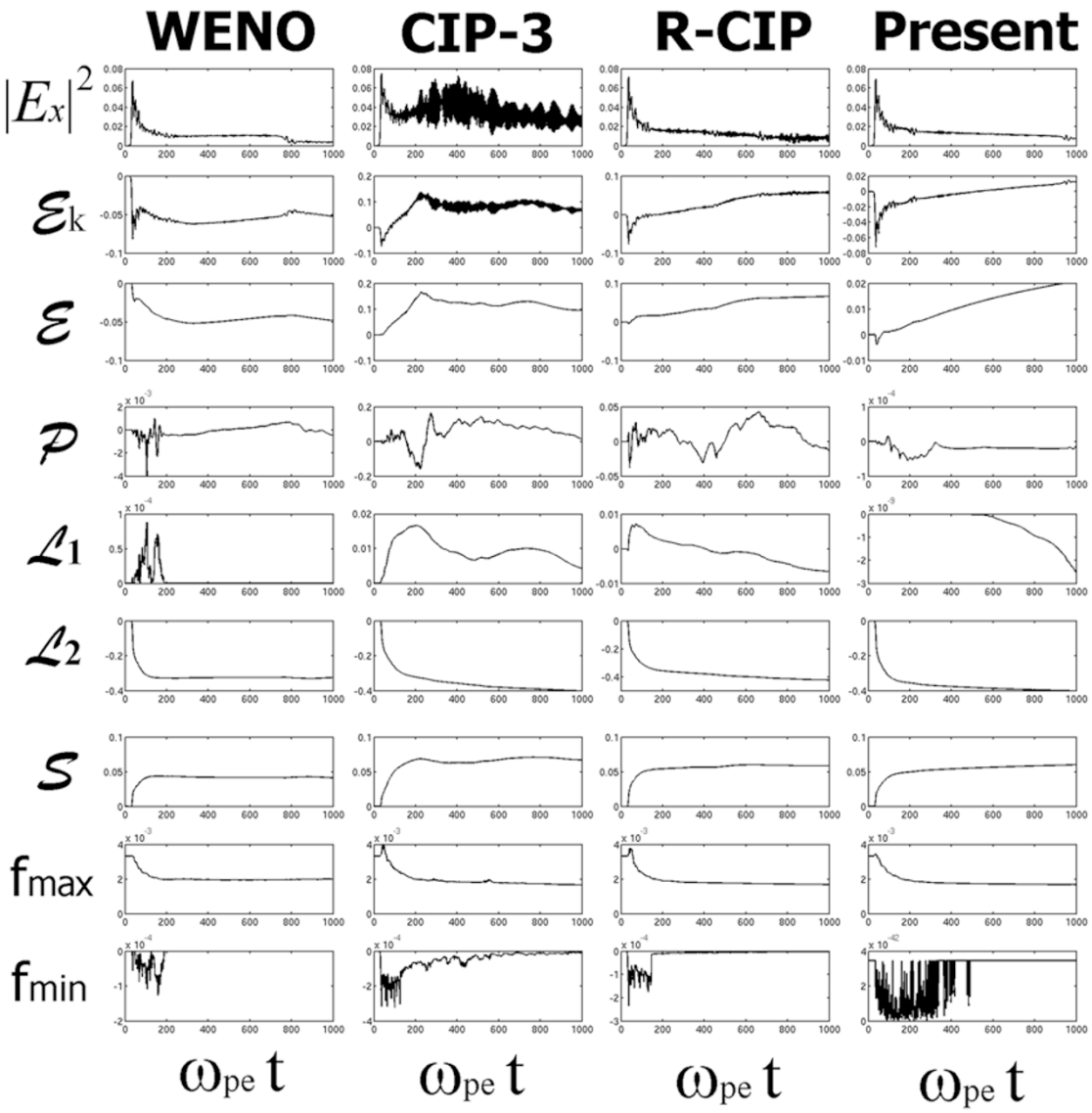

Fig. 5. Time histories of electric field energy ($|E_x|^2$), kinetic energy ($\mathcal{E}_k$), total energy ($\mathcal{E}$), momentum ($\mathcal{P}$), total density (L1 norm) ($\mathcal{L}_1$), L2 norm ($\mathcal{L}_2$), entropy ($\mathcal{S}$), the maximum and the minimum values of the distribution function, (f_{max} and f_{min}) obtained with the WENO, CIP, R-CIP, and the present schemes. The quantities $\mathcal{E}_k$, $\mathcal{E}$, $\mathcal{L}_1$, $\mathcal{L}_2$, and $\mathcal{S}$ are plotted as deviations from the initial values. The momentum, L1 and L2 norms, and entropy are normalized by their initial values, whereas the energy quantities are normalized by the initial total energy.

Table 1. CPU time for each run.

	MUSCL	WENO	CIP-3	R-CIP	Present
Time (sec)	2120.1	7221.4	4105.7	5569.7	1656.5

servations.

Since the present scheme is also a non-oscillatory scheme, we can completely remove the non-physical instability due to the numerically generated positive gradient in the velocity distribution function. We can also keep the density conservation with the present scheme because the positivity of the distribution function is achieved. The total density (L1 norm) slightly decreases in time due to the open boundaries in the v direction. Note that the present scheme is the most diffusive in the high-resolution schemes used in the present study. Thus, the saturation level of the electric field is lower than that with the WENO, CIP-3, and R-CIP schemes. Nevertheless, the present scheme provides the best result for the energy and momentum conservations. However, the history of entropy shows monotone increasing in the late nonlinear stage ($\omega_{pe}t > 400$) due to the high-numerical diffusion, whereas the history of entropy shows saturation with the WENO, CIP, and R-CIP schemes. This means that the cubic polynomial interpolant used in the present scheme is not enough, and we need to develop a higher-order scheme.

Finally, CPU loading of the schemes is discussed. Table 1 shows the CPU time of entire simulation run ($\omega_{pe}t = 0 \sim 1000$). The CPU time is measured on a single Intel Core 2 processor. The present scheme works as fast as the MUSCL scheme, in which the third order numerical flux is computed with several "IF" statements. The CIP-type schemes need more CPU time than the present scheme because the former

schemes update $\frac{\partial f}{\partial x}$ and $\frac{\partial f}{\partial v}$ as well as f. The WENO scheme reconstructs the fifth-order non-oscillatory flux from the third-order numerical flux, which needs much more CPU time than other schemes.

4. Discussion and Conclusion

For classical problems of plasma physics, such as the linear growth and saturation of an instability, there is no critical difference between the results with all the high-resolution schemes used in the present study. On the other hand, for a long-time and highly nonlinear problem, the present scheme appears to be more efficient although it is somewhat more diffusive than the other schemes.

The present benchmark test suggests that it is important for conservation laws to preserve the positivity of the distribution functions. Another important point is the suppression of numerical diffusion, by which a velocity distribution function becomes wider in velocity space. Due to the numerical modification of velocity distribution function, the following non-physical effects appear: (1) Growth rates of unstable wave modes become lower; (2) The saturation level of field energy becomes lower; (3) The total energy increases numerically. The effects (1) and (2) lower the electric field energy at the saturation state, whereas effect (3) increases the total energy in the long-time nonlinear evolution. To suppress numerical diffusion, we need enough resolution in both velocity and configuration spaces or we need schemes of a much higher order.

In conclusion, we have developed a new non-oscillatory, positive, and conservative scheme for Vlasov code simulations, which would be named as "PIC" scheme (where "PIC" stands for Positive Interpolation for Conservations). The present scheme was implemented by the author in the 1D electrostatic Vlasov code. It was used for the simulations of nonlinear beam-plasma interactions (Umeda, 2006, 2007; Ryu *et al*., 2007). It is noted that application of the present scheme should not be limited to Vlasov codes. Implementation of the present scheme to MHD, Hall-MHD, and multi-fluid codes is currently being undertaken (e.g., Tanaka *et al*., 2008).

It is also noted there have been a number of recent attempts to implement advanced numerical techniques, such as an unstructured grid system (Besse and Sonnendrucker, 2003), an adaptive multi-scale grid system (Gutnic *et al*., 2004), or a moving grid system (Sonnendrucker *et al*., 2004; Yabe *et al*., 2004). These techniques are useful to suppress numerical diffusion. However, these are beyond the scope of this paper and remain to be discussed in future research.

Acknowledgments. This work was supported by Grant-in-Aid for Young Scientists (Start-up) #19840024 from JSPS and in part by Grant-in-Aid for Creative Scientific Research #17GS0208 "The Basic Study of Space Weather Prediction" from MEXT of Japan. This work was also carried out as a collaborative computational research project at Solar-Terrestrial Environment Laboratory, Nagoya University.

References

Arber, T. D. and R. G. L. Vann, A critical comparison of Eulerian-grid-based Vlasov solvers, *J. Comput. Phys.*, **180**, 339–357, 2002.

Besse, N. and E. Sonnendrucker, Semi-Lagrangian schemes for the Vlasov equation on an unstructured mesh of phase space, *J. Comput. Phys.*, **191**, 341–376, 2003.

Cheng, C. Z. and G. Knorr, The integration of the Vlasov equation in configuration space, *J. Comput. Phys.*, **22**, 330–360, 1976.

Eliasson, B., Numerical modeling of the two-dimensional Fourier transformed Vlasov-Maxwell system *J. Comput. Phys.*, **190**, 501–522, 2003.

Elkina, N. V. and J. Buchner, A new conservative unsplit method for the solution of the Vlasov equation, *J. Comput. Phys.*, **213**, 862–875, 2005.

Filbet, F. and E. Sonnendrucker, Comparison of Eulerian Vlasov solvers, *Comput. Phys. Commun.*, **150**, 247–266, 2003.

Filbet, F., E. Sonnendrucker, and P. Bertrand, Conservative numerical schemes for the Vlasov equation, *J. Comput. Phys.*, **172**, 166–187, 2001.

Gagne, R. R. J. and M. M. Shoucri, A splitting scheme for the numerical solution of a one-dimensional Vlasov equation, *J. Comput. Phys.*, **24**, 445–449, 1977.

Godunov, S. K., A difference scheme for numerical solution of discontinuous solution of hydrodynamic equations, *Math. Sbornik*, **47**, 271–306, 1959.

Gutnic, M., M. Haefele, I. Pauna, and E. Sonnendrucker, Vlasov simulations on an adaptive phase-space grid, *Comput. Phys. Commun.*, **164**, 214–219, 2004.

Klimas, A. J., Numerical method based on the Fourier-Fourier transform approach for modeling 1-D electron plasma evolution, *J. Comput. Phys.*, **50**, 270–306, 1983.

Jiang, G.-S. and C.-W. Shu, Efficient implementation of weighted ENO schemes, *J. Comput. Phys.*, **126**, 202–228, 1996.

Mangeney, A., F. Califano, C. Cavazzoni, and P. Travnicek, A numerical scheme for the integration of the Vlasov-Maxwell system of equations *J. Comput. Phys.*, **179**, 495–538, 2002.

Nakamura, T. and T. Yabe, Cubic interpolated propagation scheme for solving the hyper-dimensional Vlasov-Poisson equation in phase space, *Comput. Phys. Commun.*, **120**, 122–154, 1999.

Pohn, E., M. Shoucri, and G. Kamelander, Eulerian Vlasov codes, *Comput. Phys. Commun.*, **166**, 81–93, 2005.

Ryu, C.-M., T. Rhee, T. Umeda, P. H. Yoon, and Y. Omura, Turbulent acceleration of superthermal electrons, *Phys. Plasmas*, **14**, 100701, 2007.

Schmitz, H. and R. Grauer, Darwin-Vlasov simulations of magnetized plasmas, *J. Comput. Phys.*, **214**, 738–756, 2006.

Shoucri, M. and R. R. J. Gagne, Numerical solution of the Vlasov equation by transform methods, *J. Comput. Phys.*, **21**, 238–242, 1976.

Sonnendrucker, E., J. Roche, P. Bertrand, and A. Ghizzo, The Semi-Lagrangian method for the numerical resolution of the Vlasov equation, *J. Comput. Phys.*, **149**, 201–220, 1999.

Sonnendrucker, E., F. Filbet, A. Friedman, E. Oudet, and J.-L. Vay, Vlasov simulations of beams with a moving grid, *Comput. Phys. Commun.*, **164**, 390–395, 2004.

Tanaka, S., T. Umeda, Y. Matsumoto, T. Miyoshi, and T. Ogino, Implementation of non-oscillatory and conservative scheme into magnetohydrodynamic equations, *Earth Planets Space*, 2008 (under review).

Umeda, T., Vlasov simulation of amplitude-modulated Langmuir waves, *Phys. Plasmas*, **13**, 092304, 2006.

Umeda, T., Vlasov simulation of Langmuir wave packets, *Nonlinear Proc. Geophys.*, **14**, 671–679, 2007.

Umeda, T., Y. Omura, P. H. Yoon, R. Gaelzer, and H. Matsumoto, Harmonic Langmuir waves. III. Vlasov simulation, *Phys. Plasmas*, **10**, 382–391, 2003.

Umeda, T., M. Ashour-Abdalla, and D. Schriver, Comparison of numerical interpolation schemes for one-dimensional electrostatic Vlasov code, *J. Plasma Phys.*, **72**, 1057–1060, 2006.

Utsumi, T., T. Kunugi, and J. Koga, A numerical method for solving the one-dimensional Vlasov-Poisson equation in phase space, *Comput. Phys. Commun.*, **108**, 159–179, 1998.

Xiao, F., T. Yabe, and T. Ito, Constructing oscillation preventing scheme for advection equation by rational function, *Comput. Phys. Commun.*, **93**, 1–12, 1999.

Yabe, T., F. Xiao, and T. Utsumi, The constrained interpolation profile method for multiphase analysis, *J. Comput. Phys.*, **169**, 556–593, 2001.

Yabe, T., H. Mizoe, K. Takizawa, H. Moriki, H.-N. Im, and Y. Ogata, Higher-order schemes with CIP method and adaptive Soroban grid towards mesh-free scheme, *J. Comput. Phys.*, **194**, 57–77, 2004.

Yamamoto, S. and H. Daiguji, Higher-order-accurate upwind schemes for solving the compressible Euler and Navier-Stokes equations, *Comput. Fluids*, **22**, 259–270, 1993.

T. Umeda (e-mail: umeda@stelab.nagoya-u.ac.jp)